Visualization of Parameter Sensitivity of 2D Time-Dependent Flow

Karsten Hanser[1], Ole Klein[1], Bastian Rieck[2], Bettina Wiebe[3], Tobias Selz[4], Marian Piatkowski[1], Antoni Sagristà[1], Boyan Zheng[1], Mária Lukácová-Medvidová[3], George Craig[4], Heike Leitte[5], and Filip Sadlo[1]

[1] Heidelberg University, Germany
[2] ETH Zurich, Switzerland
[3] Johannes Gutenberg University Mainz, Germany
[4] Ludwig Maximilian University of Munich, Germany
[5] University of Kaiserslautern, Germany

Abstract. In this paper, we present an approach to analyze 1D parameter spaces of time-dependent flow simulation ensembles. By extending the concept of the finite-time Lyapunov exponent to the ensemble domain, i.e., to the parameter that gives rise to the ensemble, we obtain a tool for quantitative analysis of parameter sensitivity both in space and time. We exemplify our approach using 2D synthetic examples and computational fluid dynamics ensembles.

Keywords: Visualization of flow ensembles · parameter sensitivity.

1 Introduction

There are many problems in science and engineering that exhibit parameter dependency. A prominent type of such dependency is regarding simulation parameters, such as initial and boundary conditions, model properties, and configuration of the numerical methods. In such cases, individual simulation results cannot provide a basis for reliable investigation of the underlying problem. By contrast, ensemble-based analysis, i.e., the investigation of the respective parameter spaces by means of sets of simulations, has proven successful in such situations. That is, such ensembles consist of a set of members, with each member being an individual simulation for the respective parameter value.

One intensely researched difficulty with ensemble-based analysis, is the interpretation of the results. For example, there is an increasing body of visualization literature on the analysis of ensembles, often employing clustering techniques and techniques based on distributions. The traditional approach to conduct ensemble-based analysis is to choose some interval in the respective parameter space, sample this range using a regular sampling—each sample representing a respective member—followed by (visual) analysis of the resulting ensemble. A difficulty with traditional ensemble visualization approaches is, however, that they focus on the data. That is, they focus on the members, and do not relate

these data to the ensemble domain, i.e., they do not relate them to the parameter space that gave rise to the ensemble. In this paper, in contrast, we focus on the variation of flow ensembles with respect to 1D parameter spaces.

The main contributions of this paper are:
- extension of the Lyapunov exponent concept to ensemble variation, and
- its decomposition into parameter sensitivity and spatial error growth.

2 Related Work

Closely related work groups into two main fields, which we address in the following: visualization of ensembles and uncertainty, and sensitivity analysis.

Ensemble visualization is currently one of the intensely researched topics in visualization research. Ferstl et al. [4] present streamline variability plots, and a technique for contour analysis based on correlation [5], similar to Sanyal et al. [10]. Contour distribution is addressed by Pfaffelmoser and Westermann [9]. Whitaker et al. [13] introduce contour boxplots. For related work regarding uncertainty visualization, we to refer to Bonneau et al. [1].

In the field of comparative ensemble visualization with respect to Lagrangian transport, the most closely related work is that by Hummel et al. [7]. In their work, they investigate the spatial spread of trajectories for each ensemble member individually, based on principal component analysis, and the variance of the spread of the respective spatial distribution means over all members. This enables Hummel et al. to investigate the spread of any type of ensembles, i.e., also discrete ones originating from different simulation models. On the other hand, their method cannot provide insight into the structure of the dependence with respect to parameter variation. Our approach, in contrast, provides this insight in the structure of parameter dependency, but requires ensembles that originate from variation of such a parameter. Due to our parametric representation, our approach also enables visualization of the spread over all members. Thus, our approach is somewhat complementary to the one by Hummel et al.

Concerning sensitivity analysis, Chen et al. [3] provide analysis with respect to errors stemming from interpolation in time-varying data. McLoughlin et al. [8] focus on visualizing the effects of parameter perturbations by means of the geometry of pathlines. In a similar vein, Chandler et al. [2] analyze errors that arise from different pathline tracing methods. Nevertheless, none of these techniques addresses sensitivity in ensemble parameter space.

3 Method

The subject of our analysis are time-dependent flow ensembles, where each member j of the ensemble is a continuous vector field

$$\mathbf{u}^j(\mathbf{x},t) = \left(u_1^j(\mathbf{x},t),\ldots,u_n^j(\mathbf{x},t)\right)^\top, \tag{1}$$

with position $\mathbf{x} := (x_1, \ldots, x_n)^\top \in \Omega \subseteq \mathbb{R}^n$, time t, and vector component u_i^j of member j along axis of x_i, i.e., $j \in \mathbb{R}$ also represents the ensemble parameter. This leads to the *ensemble domain* $\overline{\Omega} \subseteq \mathbb{R}^n \times \mathbb{R}$, *space-parameter position*

$$\overline{\mathbf{x}} = (\mathbf{x}^\top, j)^\top := (x_1, \ldots, x_n, j)^\top \in \overline{\Omega}, \tag{2}$$

and the continuous *ensemble vector field*

$$\overline{\mathbf{u}}(\overline{\mathbf{x}}, t) := \Big(u_1^j(\mathbf{x}, t), \ldots, u_n^j(\mathbf{x}, t), 0\Big)^\top \in \overline{\Omega}. \tag{3}$$

Following the finite-time Lyapunov exponent (FTLE) approach by Haller [6], we base our approach on the flow map $\boldsymbol{\phi}_{t_0}^T(\mathbf{x})$, which maps the seed $\mathbf{x}$ of a pathline $\boldsymbol{\xi}_{t_0}^{\mathbf{x}}(t)$ started at time t_0 to its endpoint after advection for time T, i.e.,

$$\boldsymbol{\phi}_{t_0}^T(\mathbf{x}) = \big(\phi_{t_0,1}^T(\mathbf{x}), \ldots, \phi_{t_0,n}^T(\mathbf{x})\big)^\top := \boldsymbol{\xi}_{t_0}^{\mathbf{x}}(t_0 + T), \tag{4}$$

with $\boldsymbol{\xi}_{t_0}^{\mathbf{x}}(t_0) := \mathbf{x}$, and $\phi_{t_0,i}^T$ being the i^{th} component of the flow map. For traditional vector fields, the FTLE is defined from this by

$$\sigma_{t_0}^T(\mathbf{x}) := \frac{1}{|T|} \ln \left\| \nabla \boldsymbol{\phi}_{t_0}^T(\mathbf{x}) \right\|_2, \tag{5}$$

with $\| \cdot \|_2$ being the spectral matrix norm, i.e., for a matrix A, the square root of the largest eigenvalue of $A^\top A$.

In our ensemble field setting, this leads to the *ensemble flow map* $\overline{\boldsymbol{\phi}}_{t_0}^T(\overline{\mathbf{x}})$ that maps a space-parameter start point $\overline{\mathbf{x}}$ of a (purely spatial) pathline seeded at $\mathbf{x}$ and time t_0 in member j to its space-parameter endpoint

$$\overline{\boldsymbol{\phi}}_{t_0}^T(\overline{\mathbf{x}}) := \big(\boldsymbol{\phi}_{t_0}^T(\mathbf{x})^\top, j\big)^\top \tag{6}$$

after advection for time T. The mapping from ② to ②' in Figure 1(a) is an example of such a trajectory within a member, and for the resulting entry in the ensemble flow map $\overline{\boldsymbol{\phi}}_{t_0}^T(\overline{\mathbf{x}})$.

3.1 Ensemble Spread

Following Equation 5, it would be straightforward to derive an ensemble finite-time Lyapunov exponent field $\overline{\sigma}_{t_0}^T(\overline{\mathbf{x}})$ from the ensemble flow map via

$$\overline{\sigma}_{t_0}^T(\overline{\mathbf{x}}) := \frac{1}{|T|} \ln \left\| \nabla \overline{\boldsymbol{\phi}}_{t_0}^T(\overline{\mathbf{x}}) \right\|_2. \tag{7}$$

However, taking a look at the Jacobian $\nabla \overline{\boldsymbol{\phi}}_{t_0}^T(\overline{\mathbf{x}})$ reveals the following structure:

$$\nabla \overline{\boldsymbol{\phi}}_{t_0}^T := \begin{pmatrix} \frac{\partial}{\partial x_1}\phi_{t_0,1}^T & \cdots & \frac{\partial}{\partial x_n}\phi_{t_0,1}^T & \frac{\partial}{\partial j}\phi_{t_0,1}^T \\ \vdots & \ddots & \vdots & \vdots \\ \frac{\partial}{\partial x_1}\phi_{t_0,n}^T & \cdots & \frac{\partial}{\partial x_n}\phi_{t_0,n}^T & \frac{\partial}{\partial j}\phi_{t_0,n}^T \\ \frac{\partial j}{\partial x_1} = 0 & \ldots & \frac{\partial j}{\partial x_n} = 0 & \frac{\partial j}{\partial j} = 1 \end{pmatrix} = \begin{pmatrix} \nabla \boldsymbol{\phi}_{t_0}^T & \frac{\partial}{\partial j}\boldsymbol{\phi}_{t_0}^T \\ \mathbf{0}^\top & 1 \end{pmatrix}. \tag{8}$$

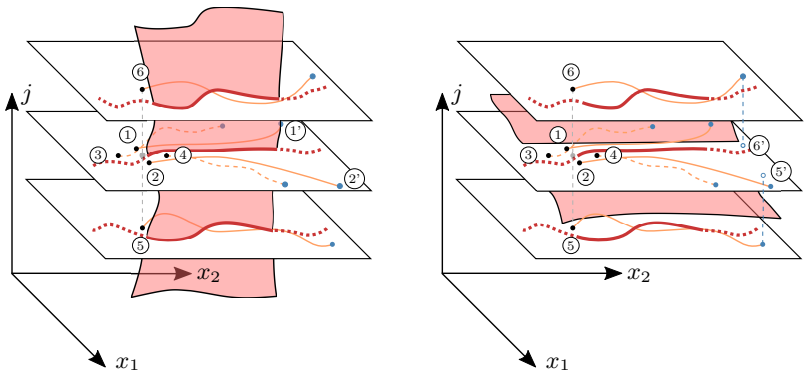

Fig. 1. Ensemble vector field of 2D members in 3D ensemble domain ($x_1 \times x_2 \times j$). (a) ES-FTLE ${}^{s}\sigma^{T}_{t_0}(\overline{\mathbf{x}})$ measures spatial separation (①'–②') with respect to spatial perturbation (in x_i, ①–②), and thus predictability and topology of trajectories (red manifold). (b) EP-FTLE ${}^{p}\sigma^{T}_{t_0}(\overline{\mathbf{x}})$ measures spatial separation (⑤'–⑥') with respect to parametric perturbation (in j, ⑤–⑥), and thus parameter sensitivity (red manifold).

We identify an upper left block, which has unit 1 because the flow map is derived with respect to the input coordinate, and an upper right block, which has generally a different unit: the unit of the coordinates x_i divided by the unit of j. Thus, $\overline{\sigma}^{T}_{t_0}$ has no direct utility/interpretation, and is influenced by the "scaling" between the different units, which could be, in general, chosen arbitrarily. Additionally, it would measure the combined spread in x_i and j with respect to x_i and j, meaning that the Euclidean distance factor for the respective endpoints in the ensemble domain $\overline{\Omega}$ would be larger or equal than 1 (since, as can be seen from Equation 3, trajectories cannot approach or deviate in j-direction). These circumstances motivate us to decompose $\nabla\overline{\boldsymbol{\phi}}^{T}_{t_0}$ into these two blocks.

3.2 Ensemble-Space Finite-Time Lyapunov Exponent

The upper left block in Equation 8 represents the traditional (purely spatial) flow map gradient, as used for traditional FTLE computation (Equation 5), although with the difference that it is now a field in the entire $(n+1)$-dimensional ensemble domain $\overline{\Omega}$, i.e., we have $\nabla\boldsymbol{\phi}^{T}_{t_0}(\overline{\mathbf{x}})$ instead of $\nabla\boldsymbol{\phi}^{T}_{t_0}(\mathbf{x})$, leading to the ensemble-space finite-time Lyapunov exponent (ES-FTLE) field

$$ {}^{s}\sigma^{T}_{t_0}(\overline{\mathbf{x}}) := \frac{1}{|T|} \ln \left\| \nabla\boldsymbol{\phi}^{T}_{t_0}(\overline{\mathbf{x}}) \right\|_2 \tag{9} $$

in the ensemble domain. This field captures, for each space-parameter point $\overline{\mathbf{x}}$, the amount of *spatial* separation of trajectories started in the *spatial* vicinity of $\mathbf{x}$ in member j. In Figure 1(a), the increase of the distance between ① and ② before advection to the distance between ①' and ②' after advection illustrates this. On the one hand, this traditional (spatial) FTLE in the ensemble

domain enables us to analyze predictability, i.e., error growth with respect to the seed *position* of a trajectory. On the other hand, it also enables us to reveal the spatial time-dependent topology [12] by extracting Lagrangian coherent structures (LCS) in terms of height ridges therefrom [11], which separate spatial regions of qualitatively different spatial behavior. Since our ensemble domain is $(n{+}1)$-dimensional, the respective $(n{-}1)$-dimensional ridges (lines in case of $n = 2$) in Ω are present as n-dimensional ridges (surfaces in case of $n = 2$) in $\overline{\Omega}$. Since in our work the focus is on parameter sensitivity and not topology, we visualize the resulting fields with volume rendering instead of extracting ridges.

3.3 Ensemble-Parameter Finite-Time Lyapunov Exponent

The upper right block in Equation 8 represents the partial derivative of the flow map with respect to the ensemble parameter j. We use it to derive the ensemble-parameter finite-time Lyapunov exponent (EP-FTLE) field

$$ {}^{p}\sigma^{T}_{t_0}(\overline{\mathbf{x}}) := \frac{1}{|T|} \ln \left\| \frac{\partial}{\partial j} \boldsymbol{\phi}^{T}_{t_0}(\overline{\mathbf{x}}) \right\|_2 . \tag{10} $$

Since $\partial \boldsymbol{\phi}^{T}_{t_0} / \partial j$ is a $n \times 1$ matrix, we may interpret it as a vector that linearizes the flow map. Hence, its spectral norm is simply the Euclidean norm. The EP-FTLE represents, for each position $\overline{\mathbf{x}} \in \overline{\Omega}$, the amount of *spatial* separation of trajectories started at position $\mathbf{x}$ in the *parametric* vicinity of member j. In Figure 1(b), the growth of the distance between ⑤ and ⑥ before advection to the distance between ⑤' and ⑥' (the spatial projection of the endpoints after advection) represents this quantity (note that the distance between ⑤ and ⑥ is illustrated too large for clarity, it is intrinsically identical to the distance between ① and ②). The EP-FTLE represents the Lagrangian parameter sensitivity of the ensemble j at position $\mathbf{x}$ and time t_0 with respect to perturbation of j. Thus, regions in $\overline{\Omega}$, where the EP-FTLE is low, are not subject to substantial change if j is varied. A possible consequence is that such regions do not need to be explored at higher resolution with respect to j. On the other hand, in regions with a high EP-FTLE, the choice of j has large impact on the result and thus needs to be carefully investigated.

Notice that the (ES-)FTLE is a logarithmic measure representing a rate of particle separation. Since it is widely used for qualitative (topological) analysis, the logarithm is not an issue in visualization. However, we present our EP-FTLE for quantitative analysis of parameter sensitivity. Therefore, in our visualizations, we omit the logarithm in Equation 10.

Notice also that our approach is basically applicable to *any* number of ensemble parameters, i.e., it supports an m-dimensional vector $\mathbf{j}$ instead of a scalar parameter j. In this case, the upper right block in Equation 8 is a matrix $\nabla_{\mathbf{j}} \boldsymbol{\phi}^{T}_{t_0}$, which can be evaluated in Equation 10 with the spectral matrix norm. In cases where all m parameters have the same unit, the result is well-defined and directly interpretable. Nevertheless, we do not exemplify such cases for two main reasons: First, direct visualizations of $\overline{\Omega}$ are infeasible in general because they

exceed three dimensions. The more important reason is, however, that different parameters typically have different units. As we argue in this paper, mixing those units may lead to interpretation difficulties. Our technique would be able to visualize the impact of each parameter individually, though. We leave the problem of handling multiple parameters as future work.

4 Results

We employ our technique to a set of synthetic and simulated 2D flow ensembles of increasing complexity. The first synthetic ensembles serve for an introduction and illustration of the properties of our technique. The remaining examples include cases from computational fluid dynamics (CFD) and meteorology—a field in which ensemble simulation plays a predominant role.

4.1 Saddle

We start with a simple synthetic stationary (time-independent) 2D flow ensemble that exhibits trajectory separation:

$$\overline{\mathbf{u}}(\overline{\mathbf{x}}) = \begin{pmatrix} -\sin(x)\cos(y) \\ \sin(y)\cos(x) \\ 0 \end{pmatrix} \tag{11}$$

in the domain $\overline{\Omega} = [-0.5, 0.5] \times [-0.5, 0.5] \times [-0.5, 0.5]$. This vector field represents the region around the origin of the Double Gyre example [11] in standard configuration. As can be seen, this ensemble does not vary in (is not a function of) j, i.e., all members are identical. It exhibits saddle-type nonlinear dynamics, which are captured by the traditional FTLE.

Figure 2(a) illustrates the ensemble and provides the respective ES-FTLE result with $T = 100$, sampled within $\overline{\Omega}$ at a resolution of $400 \times 400 \times 200$ nodes. One can nicely observe the high ES-FTLE values representing a ridge surface in $\overline{\Omega}$ (yellow in Figure 2(a)). This ridge surface represents a spatial (traditional) LCS that illustrates the bifurcation due to the saddle-type flow, i.e., it separates the two regions of $\overline{\Omega}$. Since there is no variation of $\overline{\mathbf{u}}(\overline{\mathbf{x}})$ in j-direction, the EP-FTLE field is constant zero in this case and thus not investigated.

4.2 Rotation

As a complement to the Saddle example, we now investigate a stationary field that does not exhibit variation in space Ω within the members j, but instead exhibits variation across the members, i.e., in j-direction:

$$\overline{\mathbf{u}}(\overline{\mathbf{x}}) = \begin{pmatrix} \cos\left(\frac{\pi}{4}\left(\tanh(5\pi j) + 1\right)\right) \\ \sin\left(\frac{\pi}{4}\left(\tanh(5\pi j) + 1\right)\right) \\ 0 \end{pmatrix} \tag{12}$$

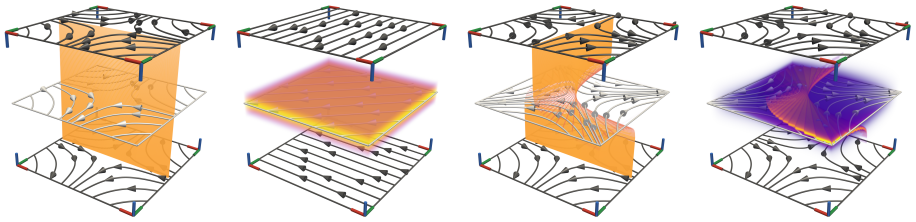

(a) (b) (c) (d)

Fig. 2. Synthetic steady flow examples (here, and in all figures: x-axis red, y-axis green, j-axis blue, and ES/EP-FTLE low value blue and high value yellow). Saddle (a) exhibits ridge (yellow) in ES-FTLE ${}^{s}\sigma_{t_0}^{T}(\overline{\mathbf{x}})$ but zero EP-FTLE ${}^{p}\sigma_{t_0}^{T}(\overline{\mathbf{x}})$. Rotation (b) exhibits zero ES-FTLE but our EP-FTLE clearly shows high parametric variation (yellow ridge) at the center of the parameter interval. In the Rotating Saddle example, ${}^{s}\sigma_{t_0}^{T}(\overline{\mathbf{x}})$ (c) shows spatial separation but fails to capture parametric variation (see separated orange lines at the center of the parameter interval). In contrast, our ${}^{p}\sigma_{t_0}^{T}(\overline{\mathbf{x}})$ (d) captures ensemble variation well, but does not capture spatial separation. Thus, ES-FTLE provides qualitative insight into the (topological) organization of flow ensembles, while the EP-FTLE is a quantitative measure for ensemble variation, i.e., parameter sensitivity.

in the domain $\overline{\Omega} = [-0.5, 0.5] \times [-0.5, 0.5] \times [-0.5, 0.5]$. Each member of this ensemble is a uniform 2D vector field with magnitude one. The direction, however, varies with member parameter j according to the hyperbolic tangent, i.e., the angle does vary very slowly at $j = -0.5$ and $j = 0.5$ and most of the range, except for $j \approx 0$, where it changes fast. As a result, the parameter sensitivity of the members is overall low with a peak at $j = 0$.

Figure 2(b) illustrates the ensemble and depicts the EP-FTLE result with $T = 100$. One can see that in this case, the EP-FTLE exhibits a ridge surface in $\overline{\Omega}$ at $j = 0$. This visualizes that the strongest member variation, i.e., largest parameter sensitivity, is at $j = 0$, and that the high EP-FTLE values separate the two regions that are qualitatively similar and exhibit small parameter sensitivity. Since the individual members represent uniform flow, the ES-FTLE is trivially constant in this case and thus not investigated.

4.3 Rotating Saddle

The third and last simple example for introducing our approach, consists of a combination of the Saddle (Section 4.1) and Rotation (Section 4.2) examples. That is, we have the flow from the Saddle example, but in this case the members undergo the same rotation as they did in the Rotation example:

$$\overline{\mathbf{u}}(\overline{\mathbf{x}}) = R(-\alpha) \begin{pmatrix} -\sin(x')\cos(y') \\ \sin(y')\cos(x') \\ 0 \end{pmatrix}, \quad R(\theta) = \begin{pmatrix} \cos(\theta) & -\sin(\theta) & 0 \\ \sin(\theta) & \cos(\theta) & 0 \\ 0 & 0 & 1 \end{pmatrix}, \tag{13}$$

with rotated space-parameter position $\overline{\mathbf{x}}' = (x', y', j)^{\top} := R(\alpha)\,\overline{\mathbf{x}}$, rotation angle $\alpha = \frac{\pi}{4}(\tanh(5\pi j) + 1)$, rotation matrix $R(\theta)$, and domain $\overline{\Omega} = [-0.5, 0.5] \times$

$[-0.5, 0.5] \times [-0.5, 0.5]$. It exhibits both a spatial separation (due to the Saddle component), and a parametric separation (due to the Rotation component). Figure 2(c) and (d) show the respective ES-FTLE and EP-FTLE.

The ridge surface (high values) in the ES-FTLE (Figure 2(c)) represents the LCS that still separates two spatial regions, however, now it is deformed due to the rotation. Furthermore, we can observe that the ES-FTLE suffers severely from aliasing, i.e., at $j \approx 0$, the LCS surface degrades into lines, which do not partition $\overline{\Omega}$. In contrast, the EP-FTLE field (Figure 2(d)) does not indicate the spatial sensitivity, but instead depicts very well (without aliasing issues) the high parameter sensitivity around $j = 0$, i.e., the high EP-FTLE values separate the two regions of $\overline{\Omega}$ with low parameter sensitivity.

4.4 Pulsating Injector

This CFD example brings us now to time-dependent simulation ensembles. It examines the injection of pulsating flow, e.g., in the context of gas injection for combustion, and consists of a 2D channel, with inflow on the left, outflow on the right, no-slip boundaries on top and bottom, and an injector inlet at the bottom left with time-dependent inflow behavior. The injector's velocity magnitude pulsates with a temporal sine. In this study, the pulsation frequency is the ensemble parameter to be examined, and is investigated in the interval $[0, 7]$, resulting in the domain $\overline{\Omega} = [0, 0.2] \times [0, 0.1] \times [0, 7]$, sampled on a grid of $800 \times 400 \times 568$.

Computing the space-parameter flow map with reverse advection time $T = -0.1$ reveals that parameter sensitivity is particularly high for low frequencies (Figure 3(a)). We select a fixed position (curve in parameter space) and start a pathline at this position in every 9^{th} member, resulting in a "parameter pathline rake". Additionally, we map the EP-FTLE to the parameter curve, revealing that high EP-FTLE values separate parameter ranges with qualitatively different pathline behavior. In contrast, the ES-FTLE (Figure 3(b)), which captures the spatial separation, does not provide such a quantitative property: it tends to be lower than the EP-FTLE at low frequencies but higher than the EP-FTLE at higher frequencies, although the pathlines do not exhibit high separation with respect to parameter variation there.

4.5 Rising Bubble

This example represents a simulation of free convection of a smooth warm air bubble surrounded by cold air, from a meteorological study, based on the Euler equations of gas dynamics. In this example, the potential temperature variation was examined by ensemble simulation. The potential temperature variation represents the deviation of the air bubble potential temperature from background equilibrium, and in this ensemble it was sampled at 31 equidistant points in the interval [0.401, 0.599]. We discretized the computational domain $\overline{\Omega} = [0, 1500]^2 \times [0.401, 0.599]$ to a grid of $1500 \times 1500 \times 31$ nodes for our analysis.

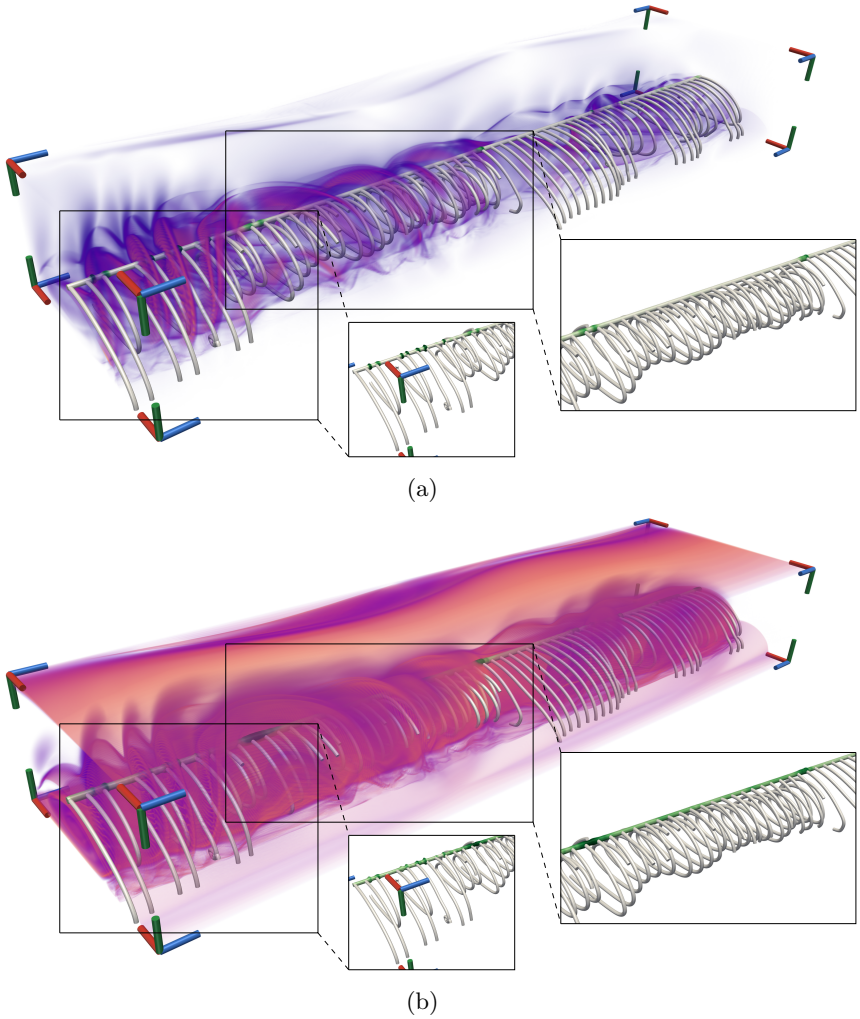

Fig. 3. Pulsating Injector example, with injection frequency increasing from left to right (blue axis). (a) EP-FTLE reveals regions of high parameter sensitivity. EP-FTLE mapped to radius and green saturation along the pathline seed "rake" reveals that large EP-FTLE quantitatively separates parameter regions with different pathline behavior. ES-FTLE (b) does not provide such quantitative view on parameter sensitivity, i.e., it is not consistent with pathline behavior (here, ES-FTLE mapped to pathline rake).

We seeded the flow map trajectories at time $t_0 = 1000$ and integrated them in reverse direction for $T = -400$. Figure 4 shows our EP-FTLE result, together with a pathline rake, and the ES-FTLE. As can be seen from the pathline variation, the EP-FTLE captures high parameter sensitivity, i.e., high EP-FTLE values separate parameter regions of qualitatively different pathline behavior.

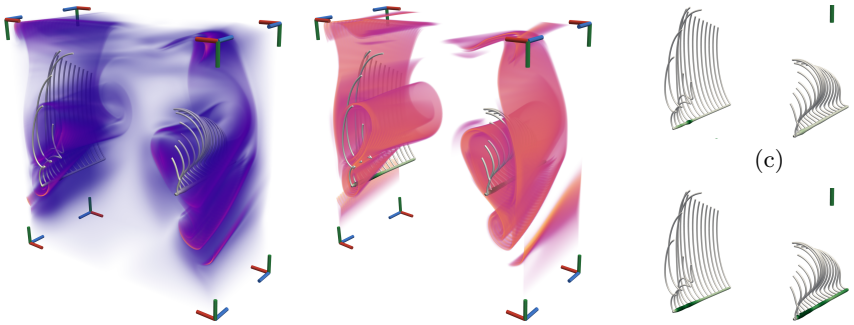

Fig. 4. Rising Bubble example, with warm air rising to the top and potential temperature, the ensemble parameter, increasing from front to back (blue axis). Quantitative visualization of parameter sensitivity by EP-FTLE (a), together with ES-FTLE (b) for comparison, and parameter pathline rake with EP-FTLE (c) and ES-FTLE (d) mapped to tube thickness and green saturation.

4.6 Rossby Waves

The large-scale atmospheric flow in the mid-latitudes is dominated by wave structures (Rossby waves), which bring polar air down to the south in their troughs and subtropical air up to the north in their ridges. The moist and warm air masses in the ridges are often forced to ascend and are referred to as Warm Conveyor Belts (WCB). The ascent leads to adiabatic cooling and to the release of latent heat by condensation and freezing of water, thus to the development of large cloud bands and to precipitation on the ground. The ridges are in general amplified by the diabatic process in WCBs through the associated upper-level divergence and vertical advection of low potential vorticity. They also pose challenges to numerical weather prediction, since the relevant quantities and processes are difficult to measure and to model. The global model ICON from Deutscher Wetterdienst (DWD) has been used to conduct a series of experiments, where the amount of the latent heat release has been modified by using different values for the enthalpy of condensation and freezing in the model. The enthalpy has been varied from 80% up to 120% of its true value in steps of 1% in this ensemble, which should lead to a damped or increased WCB activity and associated ridge amplification.

For visualization by our technique, we discretized the computational domain $\overline{\Omega} = [-\pi, \pi] \times [0, 17/36\pi] \times [0.8, 1.2]$, representing the northern hemisphere in terms of longitude and latitude times the ensemble dimension, to a grid of $2000 \times 500 \times 41$ nodes. The flow map trajectories are seeded at $t_0 = 3.6 \cdot 10^5$ s $= 100$ h and advected for $T = 1.8 \cdot 10^5$ s $= 50$ h.

For analysis, we again conduct the same steps as in the previous examples. Whereas predictability/topology by means of ES-FTLE shows many strong coherent vortex structures (Figure 5(d)), the EP-FTLE has only a few peaks. This shows that although there is a large number of topological structures identified by

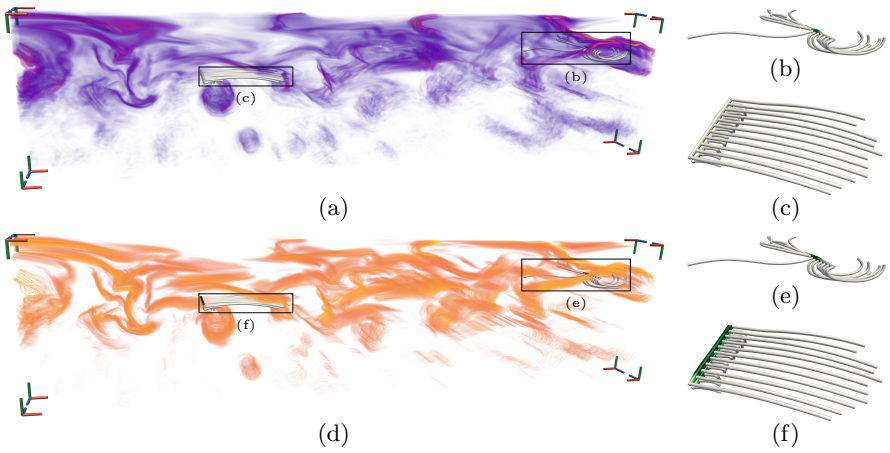

Fig. 5. Rossby Waves example, with enthalpy, the ensemble parameter, increasing from front to back (blue axis). Quantitative visualization by means of EP-FTLE (a) reveals only few regions with strong parameter sensitivity. The ES-FTLE (d), in contrast, reveals strong coherent structures also toward the equator (bottom). Parameter pathline rakes with EP-FTLE and ES-FTLE mapped to seed curve thickness and green saturation. EP-FTLE captures separation due to parameter perturbation (b), (c), whereas ES-FTLE separation only due to spatial perturbation (e), (f).

means of the ES-FTLE (Figure 5(d)), the sensitivity with respect to enthalpy in the ensemble parameter space is constrained to small subregions (orange/yellow in Figure 5(a)). This reveals that the structures closer to the equator are less parameter-sensitive than those at the polar regions. A closer investigation of the reasons and implications is, however, beyond the scope of this paper and subject to future work in meteorology.

5 Conclusion

We presented an approach to quantify and visualize parameter sensitivity for 2D time-dependent flow ensembles. We extended the concept of the finite-time Lyapunov exponent to the parameter space of ensembles, and presented a decomposition, providing a "stacked" version of the traditional finite-time Lyapunov exponent which measures predictability and which we denote ES-FTLE, and providing its counterpart, the EP-FTLE, which measures parameter sensitivity of ensembles with respect to the space-time behavior of pathlines integrated over a finite time interval.

As future work, we would like to investigate parameter sampling approaches for efficient and effective ensemble computation, and investigate related approaches for visualizing 3D time-dependent vector fields. Although our approach is applicable to multi-parameter ensembles, this would lead to higher-dimensional space-parameter domains, involving visual representation issues. Addressing these issues is also a direction for possible future work.

Acknowledgments

The research leading to these results has been done within the subproject A7 of the Transregional Collaborative Research Center SFB / TRR 165 "Waves to Weather" funded by the German Science Foundation (DFG).

References

1. Bonneau, G.P., Hege, H.C., Johnson, C.R., Oliveira, M.M., Potter, K., Rheingans, P., Schultz, T.: Overview and State-of-the-Art of Uncertainty Visualization, pp. 3–27. Springer, London (2014)
2. Chandler, J., Bujack, R., Joy, K.I.: Analysis of error in interpolation-based pathline tracing. In: EuroVis Short Paper Proceeedings (2016)
3. Chen, C., Biswas, A., Shen, H.W.: Uncertainty modeling and error reduction for pathline computation in time-varying flow fields. In: IEEE Pacific Visualization Symposium (PacificVis). pp. 215–222 (Apr 2015)
4. Ferstl, F., Bürger, K., Westermann, R.: Streamline variability plots for characterizing the uncertainty in vector field ensembles. IEEE Transactions on Visualization and Computer Graphics **22**(1), 767–776 (2016)
5. Ferstl, F., Kanzler, M., Rautenhaus, M., Westermann, R.: Visual analysis of spatial variability and global correlations in ensembles of iso-contours. Computer Graphics Forum **35**(3), 221–230 (2016)
6. Haller, G.: Distinguished material surfaces and coherent structures in three-dimensional fluid flows. Physica D **149**, 248–277 (2001)
7. Hummel, M., Obermaier, H., Garth, C., Joy, K.I.: Comparative visual analysis of Lagrangian transport in CFD ensembles. IEEE Transactions on Visualization and Computer Graphics **19**(12), 2743–2752 (2013)
8. McLoughlin, T., Edmunds, M., Tong, C., Laramee, R.S., Masters, I., Chen, G., Max, N., Yeh, H., Zhang, E.: Visualization of input parameters for stream and pathline seeding. International Journal of Advanced Computer Science and Applications (IJACSA) **6**(4), 124–135 (Apr 2015)
9. Pfaffelmoser, T., Westermann, R.: Visualizing contour distributions in 2D ensemble data. In: EuroVis Short Paper Proceedings. pp. 55–59 (2013)
10. Sanyal, J., Zhang, S., Dyer, J., Mercer, A., Amburn, P., Moorhead, R.: Noodles: A tool for visualization of numerical weather model ensemble uncertainty. IEEE Transactions on Visualization and Computer Graphics **16**(6), 1421–1430 (2010)
11. Shadden, S., Lekien, F., Marsden, J.: Definition and properties of Lagrangian coherent structures from finite-time Lyapunov exponents in two-dimensional aperiodic flows. Physica D: Nonlinear Phenomena **212**(3-4), 271–304 (2005)
12. Üffinger, M., Sadlo, F., Ertl, T.: A time-dependent vector field topology based on streak surfaces. IEEE Transactions on Visualization and Computer Graphics **19**(3), 379–392 (2013)
13. Whitaker, R.T., Mirzargar, M., Kirby, R.M.: Contour boxplots: A method for characterizing uncertainty in feature sets from simulation ensembles. IEEE Transactions on Visualization and Computer Graphics **19**(12), 2713–2722 (2013)